Mecánica Computacional Vol. XXI, pp. 148–162
S. R. Idelsohn, V. E. Sonzogni and A. Cardona (Eds.)
Santa Fe–Paraná, Argentina, October 2002

NUMERICAL SIMULATION OF CHANNEL FLOWS USING THE IMMERSED BOUNDARY METHOD

Juliano M. Arruda*, Ana L. F. Lima e Silva*, Aristeu S. Neto*, Alexandre M. Roma †

*Laboratório de Transferência de Calor e Massa e Dinâmica dos Fluidos – LTCM
Faculdade de Engenharia Mecânica
Universidade Federal de Uberlândia
Campus Santa Mônica, Uberlândia, Brasil
e-mail: jmarruda@mecanica.ufu.br, alfernandes@mecanica.ufu.br, aristeus@mecanica.ufu.br

† Instituto de Matemática e Estatística
Universidade de São Paulo
Cidade Universitária, São Paulo, Brasil
e-mail: roma@ime.usp.br

Key-words: Immersed Boundary; Moving Boundary; Force Source Term; Channel Flows

Abstract. *The Immersed Boundary Method is used to model the walls bounding flows in straight channels. In this method a force source term is added to the Navier-Stokes equations, in order to guarantee the non-slipping boundary conditions at the channel walls. The Physical Virtual Model (PVM) is used to calculate the force field, which is a methodology that has been developed by the LTCM – FEMEC research group. This methodology employs the Navier-Stokes equations to compute the interfacial force presented in the flow. Results are presented for two types of flows: Poiseuille and Couette-Poiseuille. The results (velocity and friction coefficient) are compared with analytical results.*

1. INTRODUCTION

Engineering problems involving fluids flows in complex geometries are very usual, and the major difficulty arise in how to represent the body, its moving walls and its interaction with the fluid.

The most usual approach is using Neumann and Dirichlet boundaries conditions to represent the body geometry. Therefore if the geometry is complex ones have a hard and, probably, a difficult work. This difficulty grows up if the body has a moving and deformable geometry.

Some authors have proposed different methods to treat this kind of problem. Harlow & Welch[1] proposed the Marker and Cell (MAC). In this method the fluid region in on side of the boundary is identify by markers, while the other side of the boundary, which can be fluid or solid, is identify by another marker. Peskin[2] proposed his Immersed Boundary Method, in which the interface between fluid and body is represented by a lagrangean mesh, that interacts with the flows domain, represented by an eulerian mesh. A force term added to the Navier-Stokes equation is in charge to promote the interaction between these meshes. Different ideas have been proposed to calculate this force term.

Peskin's original idea was based in Hooke's Law of Elasticity. In this model the lagrangean nodes, $\boldsymbol{X_k}$, are connected by springs of constant k >>1, to a equilibrium point $\boldsymbol{X^e}$. Goldstein *et al*.[3] proposed the Virtual Boundary Formulation. In this method the force term is obtained with the sum of inercial forces over a massless body. Both methods deals with *ad-hoc* constants, which must to be fitted for each case.

Fadlun *et al*.[4] used the Navier-Stokes equation to calculate the force term in the first external grid point, using its velocity. Therefore it is necessary an algorithm to identify the grid points that must be calculate.

Lima e Silva *et al*.[5] proposed a method named Physical Virtual Model (PVM), in which the force term is calculated over a sequence of lagrangean points using the Navier-Stokes equation.

In the present work we simulate, using the PVM, two types of internal channel flow. Preliminary results are present for Poiseuille and Couette-Poiseuille flows. The flow quantities, velocity, force and friction coefficient are presented for Re = 250 (Re is defined upon the mean velocity and the channel highness). It also presented velocities profiles and frictions coefficients comparison for different Re numbers.

2. MATHEMATICAL FORMULATION

2.1. Governing equations

It was considered an incompressible, laminar and isothermal newtonian fluid in a rectangular domain Ω. The governing equations are mass conservation and Navier-Stokes. They can be written as:

$$\vec{\nabla} \cdot \vec{V} = 0, \tag{1}$$

$$\rho\left[\frac{\partial \vec{V}}{\partial t}+\left(\vec{V}\cdot\vec{\nabla}\right)\cdot\vec{V}\right] = -\vec{\nabla}\,p+\vec{\nabla}\cdot\left[\nu\left(\vec{\nabla}\cdot\vec{V}+\vec{\nabla}^{T}\cdot\vec{V}\right)\right]+\vec{F} \tag{2}$$

where ν is the kinematic viscosity, and $\vec{F}$ is an force term, that it is explained at the next topic.

2.2. Physical virtual model

The force term $\vec{F}$, that differs from null only over the boundary, represents the eulerian force field and is given by:

$$\vec{F}(\vec{x}) = \int_{\Omega}\vec{f}(\vec{x}_k)\cdot\delta(\vec{x}-\vec{x}_k)\,d\vec{x}_k\,, \tag{3}$$

where $\vec{x}_k$ are the lagrangean grid points, $\vec{f}(\vec{x}_k)$ is the lagrangean force density e $\delta(\vec{x}-\vec{x}_k)$ is a Dirac delta function. The lagrangean force is calculated by the Navier-Stokes equation, and it can be expressed by

$$\vec{f}(\vec{x}_k) = \vec{f}_a(\vec{x}_k)+\vec{f}_i(\vec{x}_k)+\vec{f}_v(\vec{x}_k)+\vec{f}_p(\vec{x}_k), \tag{4}$$

where,

$$\vec{f}_a(\vec{x}_k) = \rho\frac{\partial\vec{V}(\vec{x}_k)}{\partial t}, \tag{5}$$

$$\vec{f}_i(\vec{x}_k) = \rho\left(\vec{V}\cdot\vec{\nabla}\right)\cdot\vec{V}(\vec{x}_k), \tag{6}$$

$$\vec{f}_v(\vec{x}_k) = -\mu\nabla^2\cdot\vec{V}(\vec{x}_k), \tag{7}$$

$$\vec{f}_p(\vec{x}_k) = \vec{\nabla}\,p(\vec{x}_k). \tag{8}$$

The above terms are named as acceleration force, inertial force, viscous force and pressure force. These terms are evaluated over the boundary, using the flow velocity and pressure field. It must be noted that over the boundary the eulerian velocity $\vec{V}(\vec{x})$ and the lagrangean velocity $\vec{V}(\vec{x}_k)$ must be equal to satisfy the non-slip condition. The velocity and pressure spatial derivatives are obtained from the flow quantities by the equations (1) and (2). Once obtained these quantities are interpolated for the grid points near the interface, as can be seen in figure (1).

The first and second velocity and pressure derivatives are solved using a second order Lagrange polynomial approximation, which can be written as

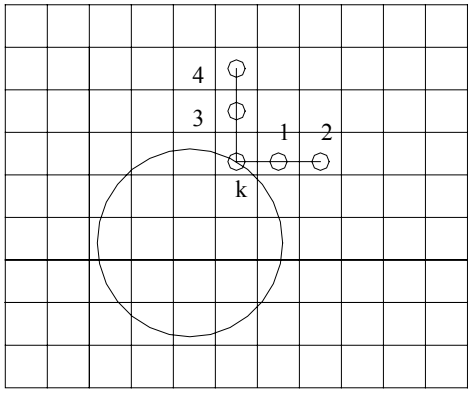

Figure 1. Interpolation scheme for velocity and pressure.

$$\frac{\partial \phi}{\partial x} = \frac{(x_i - x_k) + (x_i - x_2)}{(x_1 - x_2)(x_1 - x_k)}\phi_1 + \frac{(x_i - x_k) + (x_i - x_1)}{(x_2 - x_1)(x_2 - x_k)}\phi_2 + \frac{(x_i - x_1) + (x_i - x_2)}{(x_k - x_1)(x_k - x_2)}\phi_k , \tag{9}$$

$$\frac{\partial^2 \phi}{\partial x^2} = \frac{2\phi_1}{(x_1 - x_2)(x_1 - x_k)} + \frac{2\phi_2}{(x_2 - x_1)(x_2 - x_k)} + \frac{2\phi_k}{(x_k - x_1)(x_k - x_2)} \tag{10}$$

$$\frac{\partial \phi}{\partial y} = \frac{(y_i - y_k) + (y_i - y_4)}{(y_3 - y_4)(y_3 - y_k)}\phi_3 + \frac{(y_i - y_k) + (y_i - y_3)}{(y_4 - y_3)(y_4 - y_k)}\phi_4 + \frac{(y_i - y_3) + (y_i - y_4)}{(y_k - y_3)(y_k - y_4)}\phi_k , \tag{11}$$

$$\frac{\partial^2 \phi}{\partial y^2} = \frac{2\phi_3}{(y_3 - y_4)(y_3 - y_k)} + \frac{2\phi_4}{(y_4 - y_3)(y_4 - y_k)} + \frac{2\phi_k}{(y_k - y_3)(y_k - y_4)} . \tag{12}$$

Once calculated, the lagrangean force density is distributed to the nearest eulerian grid points, as can be seen in figure (2), by a distribution function D_{ij}. Then the equation (3) takes the form

$$\vec{F}_{ij} = \sum D_{ij}\, \vec{f}_k . \tag{13}$$

Juric[6] suggested that D_{ij} could be given by

$$D_{ij}(\vec{x}_k) = \frac{f[(x_k - x_i)/h]\, f[(y_k - y_j)/h]}{h^2} , \tag{14}$$

$$f(r) = \begin{cases} f_1(r) & se \quad \|r\| < 1 \\ \frac{1}{2} - f_1 \cdot (2 - \|r\|) & se \quad 1 < \|r\| < 2 \\ 0 & se \quad \|r\| > 2 \end{cases} , \tag{15}$$

with

$$f_1(r) = \frac{3 - 2\cdot\|r\| + \sqrt{1 + 4\cdot\|r\| - 4\cdot\|r\|^2}}{8}\ , \tag{16}$$

where r is $(x_k - x_i)/h$ or $(y_k - y_i)/h$, and h is the eulerian grid size.

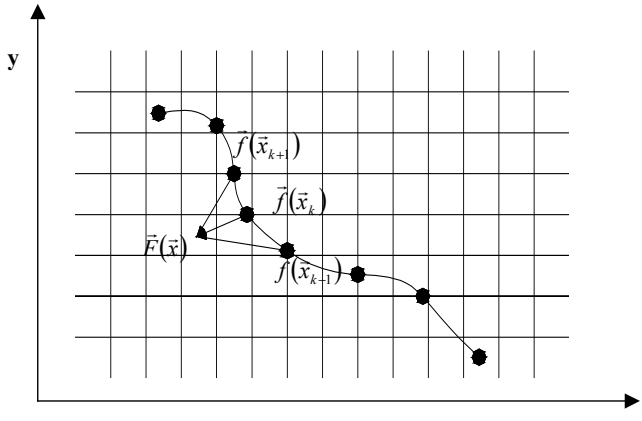

Figure 2. Force distribution process

3. NUMERICAL METHOD

Equations (1) and (2) were discretized using a central second order finite difference method in space and a Euler first order in time.

The pressure and velocity coupling was solved by a second order pressure correction method suggested by Armfield e Street[7] and the linear system was solved using the MSI, Modified Strongly Implicit Procedure, suggested by Schneider e Zedan[8].

4. RESULTS

The Immersed Boundary Method, with the Physical Virtual Model, was applied to simulate flow channels for a different Reynolds numbers in order to validate this methodology for static and moving boundaries. The channel walls were modeled using the PVM model. The physical model can be seen in figure (3). The Reynolds number is defined as a function of the height h of the channel.

The channel dimensions are $h = 0.5$, $L = 2h$. U is the upper wall velocity and Pi and Po the inflow and outflow pressure.

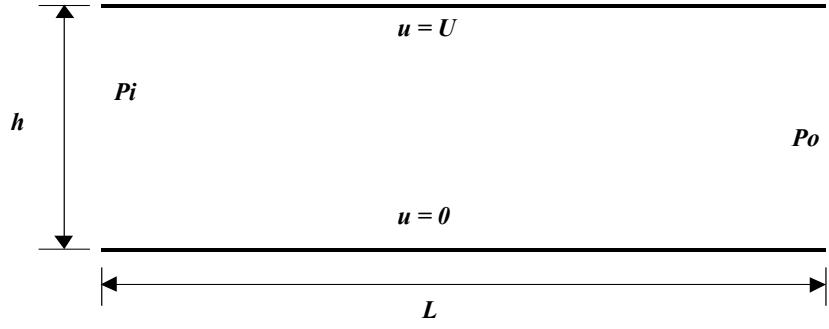

Figure 3. Channel physical model.

The Poiseuille and Couette-Poiseuille flows were simulated. The force, pressure and velocity fields for a Re = 250 are presented. It is also presented the velocity profiles and the friction coefficients as a function of Reynolds number. Comparison with analytical solutions were performed.

4.1 Poiseuille flow

The Poiseuille flow was simulated for different Re numbers. The flow conditions are listed in table 1. It is presented, for a Re = 250, the force, velocity, and pressure fields, and a comparison between the analytical and the numerical velocity profiles. The friction coefficients and velocity profiles as a function of Re number are also presented.

Table 1. Poiseuille flow conditions

Re	$Po - Pi$	ν
100	- 0,96	0,01
250	- 2,4	0,01
500	- 4,8	0,01
750	- 7,2	0,01
1000	- 9,6	0,01

Figure 4 shows the force field for Re = 250. The region where the force differs from null is the virtual wall position, modeled by the PVM model. It must be noted that when using the Immersed Boundary Method, the interface region is spread, so instead to have only one fixed value for the force, there is a range of values for it.

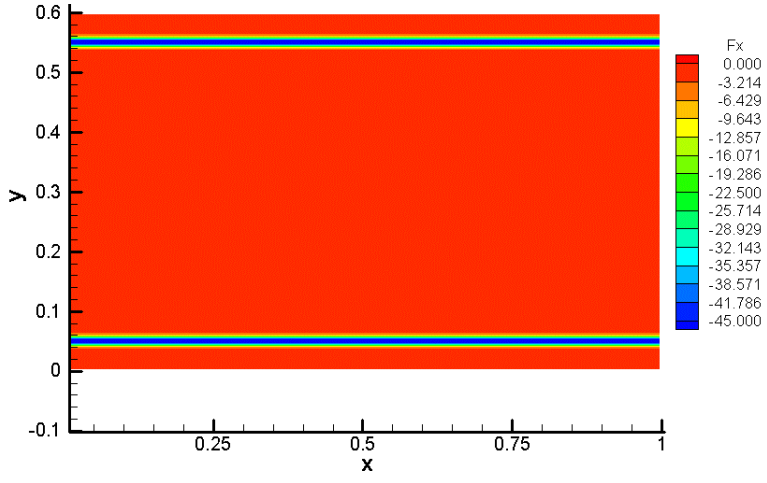

Figure 4. Force field – Re = 250

Figure 5 shows the Poiseuille flow pressure field. It can be noted the pressure dependence with the position in x direction.

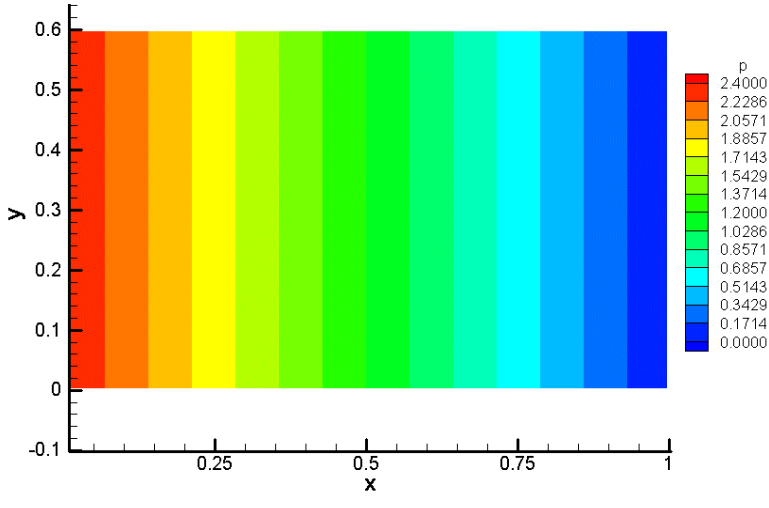

Figure 5. Pressure field – Re = 250

Figure 6 shows the velocity field. It can be seen that at the neighborhood of the virtual wall the velocity is close to null, and has a maximum in the center of the channel. The numerical

velocity result has a good agreement with the analytical one, as can be seen in figure 7. Figure 8 shows the velocity profiles as a function of the Re number, and it can be seen the pressure gradient influence in the flow. A higher pressure gradient leads to a greater velocity.

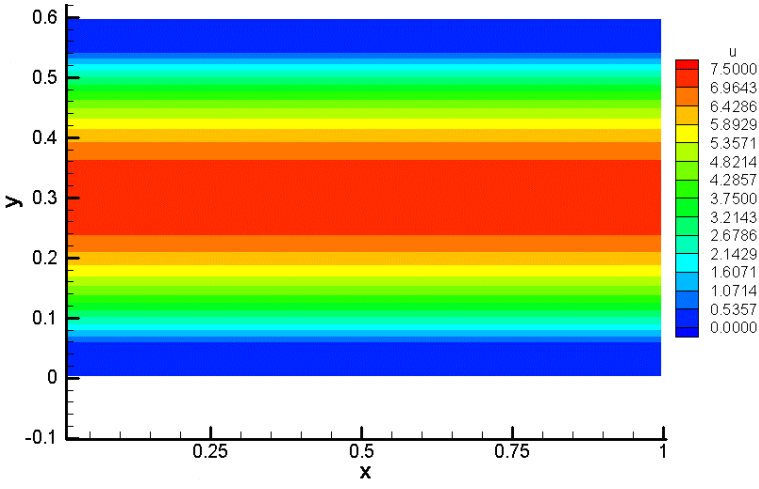

Figure 6. Velocity field – Re = 250

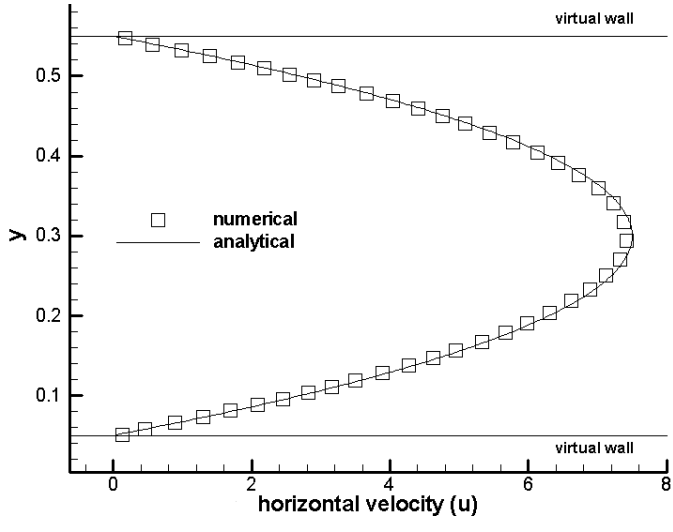

Figure 7. Numerical x analytical velocity – Re = 250

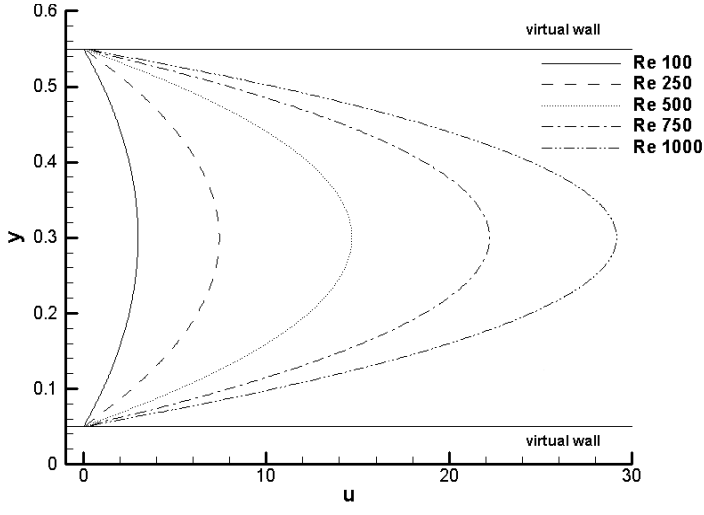

Figure 8. Velocity profiles as a function of Re number.

The numerical friction coefficient was obteined, and a comparison with the analytical coefficient was performed. The analytical friction coefficient f is defined as

$$f = \frac{\tau_{yx}}{\frac{1}{2}\rho \bar{u}^2}, \tag{17}$$

where τ_{yx} is the shear stress and $\bar{u}$ the mean velocity. The analytical shear stress is given as

$$\tau_{yx} = \mu \frac{\partial u}{\partial y}, \tag{18}$$

The numerical shear stress is calculated by multiplying the eulerian force per volume over the boundary with the grid size dx. It must be noted that in force calculation, the results are for the two sides of the wall. More clearly, there are flow at both sides of the channel wall. Thus for the analytical shear stress calculation it must be considered the flow in all domain. The friction coefficient is defined as a function of the total shear stress at the wall and the flow mean velocity in the main channel.

Figures 9 and 10 show the friction coefficients results. They are also as a function of Re number. It can be seen in figure 9 that the increasing value of the Re number leads the friction coefficients to a value closely to null. This fact is also showed in figure 10, that shows the reduction of friction coefficient as a function of Re number. The numerical friction coefficient also has a good agreement with analytical solution as can be seen in same figure.

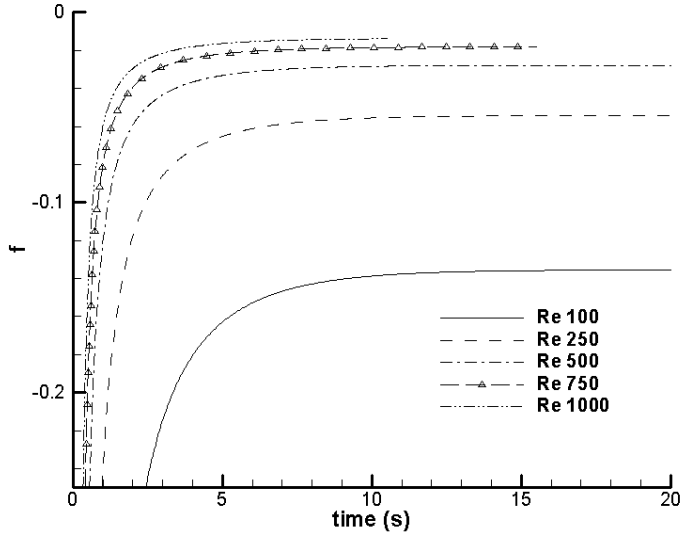

Figure 9. Friction coefficients as a function of Re number.

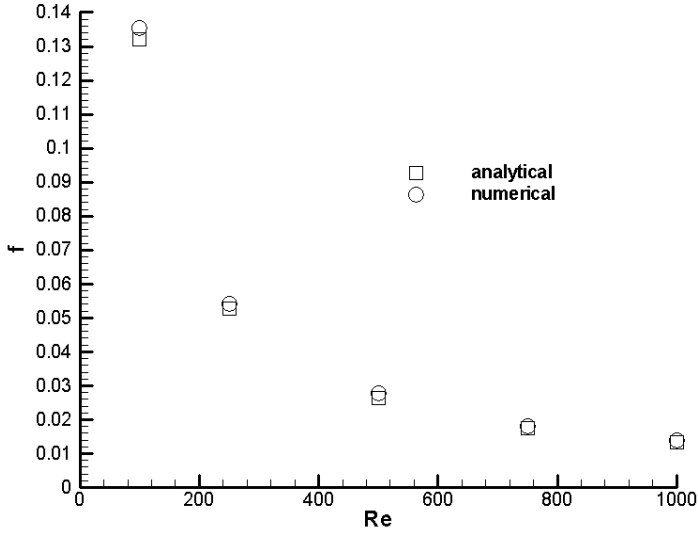

Figure 10. Friction coefficients x Re - numerical e analytical

4.2 Couette-Poiseuille flow

The Couette-Poiseuille flow was also simulated for different Re number. The flow conditions for this flow are listed in table 2. It is presented, for a Re = 250, the force, velocity, and pressure fields, and the comparison between the analytical and numerical velocity profiles. Again it is showed the friction coefficients and velocity profiles as a function of Re number.

Table 2. Couette-Poiseuille flow conditions

Re	U	$\Delta P = Po - Pi$	ν
100	1,0	- 0,72	0,01
250	1,0	- 2,16	0,01
500	1,0	- 4,56	0,01
750	1,0	- 6,96	0,01

Figure 11 shows the force field. It can be seen that as the upper wall velocity has a different value from the lower wall velocity, the force is also different, with a higher force (in modulus) at the lower wall, and a minor force at the upper wall.

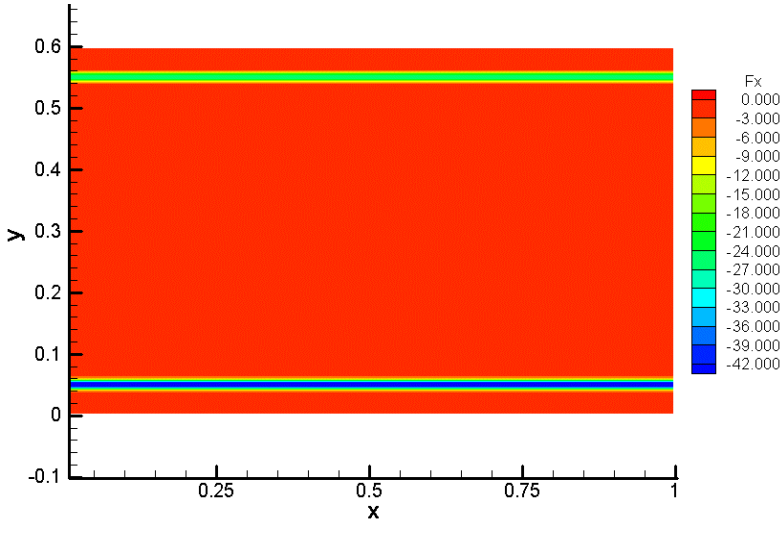

Figure 11. Force field - Re 250

The pressure field is given in figure 12. It can be noted the pressure dependence with the position in x direction.

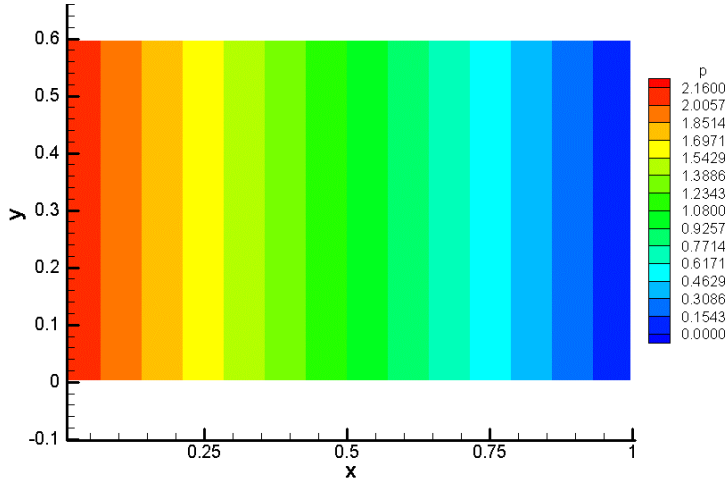

Figure 12. Pressure field - Re 250

The velocity results are shown in figures 13 and 14. The maximum velocity occurs above the central line of the channel, as could be predicted by the analytical solution. It can be noted the pressure gradient influence over the flow. As higher is the pressure gradient, more closely to a parabolic shape and less asymmetric is the velocity profile. Again there is a good agreement between the numerical and analytical results.

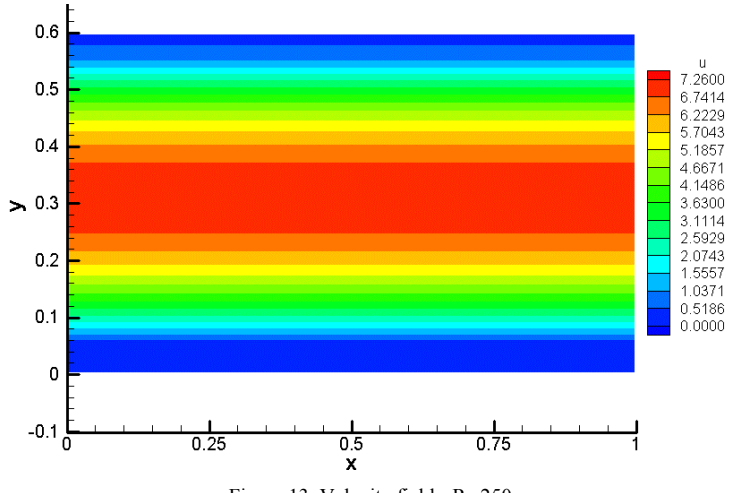

Figure 13. Velocity field - Re 250

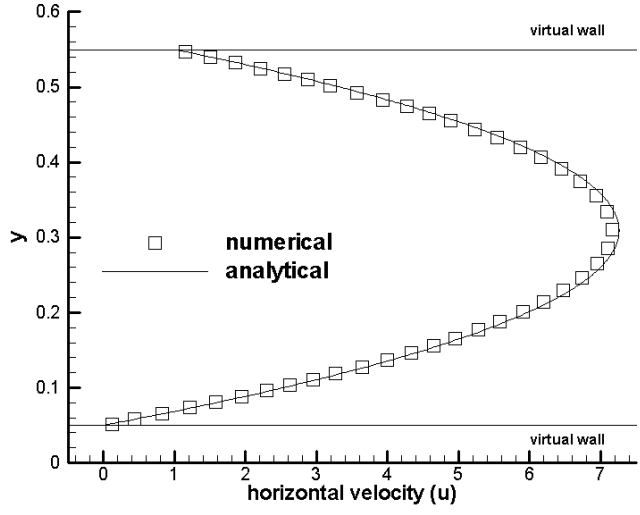

Figure 14. Numerical x analytical velocity – Re = 250

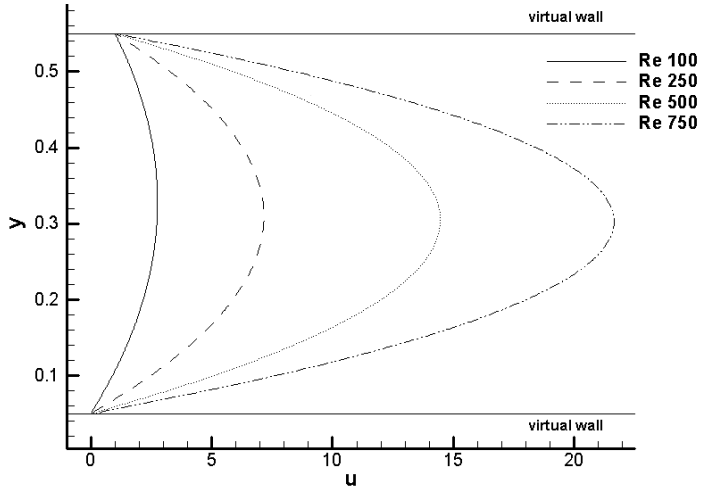

Figure 15. Velocity profiles as a function of Re number.

Figure 16 shows that in Couette-Poiseuille flow two friction coefficients are obtained. This occurs because there are two shear stress: the first due to the upper moving wall and the pressure gradient, and the other due only to the pressure gradient.

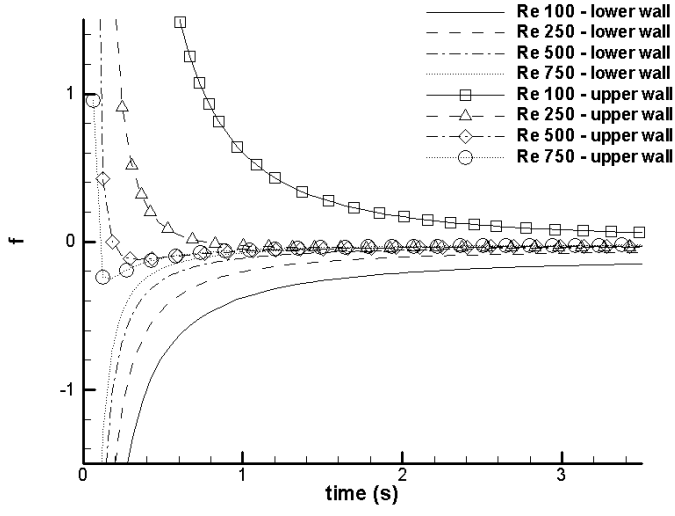

Figure 16. Friction coefficients as a function of Re number.

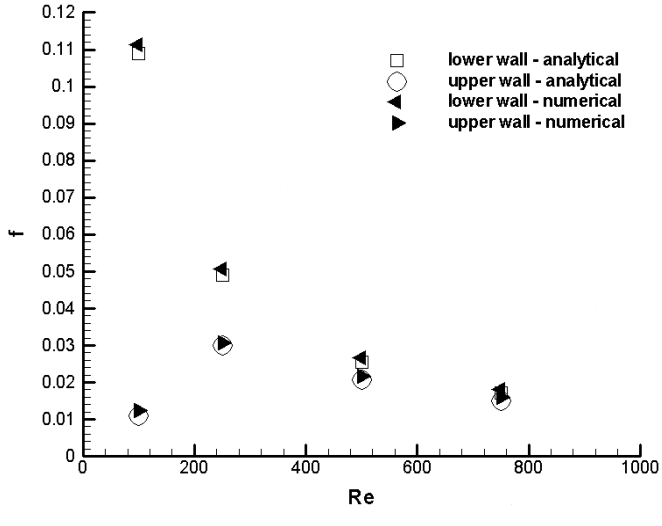

Figure 17. Friction coefficients x Re - numerical e analytical

It can be noted again in figure 17 the Re number influence over the friction coefficients. As the Re increases, both the friction coefficient decreases up to a value close to null. All the notes written to the Poiseuille flow for the friction coefficient calculation are useful to the Couette-Poiseuille flow.

5. CONCLUSIONS

The methodology proposed permits to obtain results that have good agreement with the analytical solutions.. The errors were in a order of 1%. These results permits to advance in order to implement the methodology for more complex geometries, such as cavities and flow chambers with moving boundaries.

6. ACKNOWLEDGEMENTS

This work was supported by CNPq (Brazilian Research Council).

7. REFERENCES

[1] F. H. Harlow, and J. E. Welch, "Numerical calculation of time-dependent viscous of incompressible flow of fluid with free surface", *Physics Fluids*, **8**, pp. 2182-2189, (1965).

[2] C.S Peskin, "Numerical analysis of blood flow in the heart*", Journal of. Computational Physics,* **25**,220-252, (1977).

[3] D. Goldstein, R. Hadler and L. Sirovich, "Modeling a no-slip flow boundary with an external force field", Journal of Computational Physics, **105**, 354, (1993).

[4] E. A. Fadlun, R. Verzicco, P. Orlandi, and J., Mohd-Yusof, "Combined immersed-boundary finite-difference methods for three-dimensional complex flow simulations", *Journal of Ccomputational Physics*, **161**, 35-60, 2000.

[5] A. L. F. Lima e Silva, A. Silveira-Neto, J. J. R. Damasceno, "Numerical simulation of two dimensional flows over a circular cylinder using a immersed boundary method", paper submitted to the Journal of Computational Physics.

[6] D. Juric, *Computation of phase change,* Ph.D. Thesis, Mechanical Engineering, University of Michigan, (1996).

[7] S. Armfield, and R. Street, "The fractional-step method for the navier-stokes on staggered grids: the accuracy of three variations". NOTE. *Journal of Computational Physics*, **153**, 660-665, (1999).

[8] G E. Schneider, and M. Zedan, "A modified strongly implicit procedure for the numerical solution of field problems". *Numerical Heat transfer*, **4**, 1-19, (1981).